strain
An International Journal for Experimental Mechanics

AE Monitoring and Numerical Simulation of a Two-span Model Masonry Arch Bridge Subjected to Pier Scour

S. Invernizzi, G. Lacidogna, A. Manuello and A. Carpinteri

Department of Structural Engineering & Geotechnics, Politecnico di Torino, Corso Duca degli Abruzzi 24 – 10129 Torino, Italy

ABSTRACT: A scaled model of a two-span masonry arch bridge has been built to investigate the effect of the central pile settlement because of riverbank erosion. The bridge geometry and the structural details, included the masonry bricks and mortar joints, are realized in the scale 1 : 2. The model bridge has been equipped with different Non-Destructive Testing (NDT) instruments, including accelerometers, displacement transducers LVTD, strain gages, optic fibres strain sensors and Acoustic Emissions (AE) transducers. The model bridge has been subjected to incremental settlement of the pile, which was sustained on a mobile support. The exact mechanism and temporal evolution of the pier scour has been investigated numerically and experimentally by mean of a hydraulic model. In this article, a detailed description of AE data and damage localization is provided. During the first stage of the settlement, the AE counting has been recorded. Based on the interpretation of the AE rate, it is possible to monitor the criticality of the ongoing process. In addition, thanks to the AE equipment, it has been possible to localize the main damaged zones. The statistical properties AE time series have been analysed using an estimation of the *b*-value of the Gutenberg-Richter (GR) law permitting to determine the damage level reached in the model. The damage evolution has been also interpreted numerically with the aid of a finite element programme able to predict the nucleation and propagation of fracture. In this way, some criteria for the monitoring and interpretation of full-scale structure cracking are provided for the assessment in presence of riverbank erosion phenomena.

KEY WORDS: *acoustic emissions, damage localization, numerical modelling, riverbank erosion, scale-model*

Introduction

Masonry arch bridges are extremely stiff structures, which are well suited to sustain high gravity loads but are very vulnerable with respect to differential settlements of the supports. In the case of multi-span arch bridges traversing rivers, the phenomenon preferably takes place in occasion of the flood peaks. The pier scour is one of the worst dangers for the integrity of historical bridges.

It is worth noting that the problem has a very important social impact, especially in countries like Italy that have a wide historical heritage. Consider that, even limiting the case to the northern region Piedmont, the masonry bridges are a few hundred. In recent years, different approaches have been attempted for monitoring the evolution of the phenomenon and to provide the necessary warning in the case of structural collapse. The main weak points of such techniques are that they cannot be used during the flood peaks and that they provide poor information about the overall integrity of the bridge.

In this context, structural monitoring [1] can be an effective complement to hydro-geological monitoring, because it could provide information about the propagation of damage and on the necessity of a quick intervention. The Non-Destructive Testing (NDT)-combined approach, with the use of dynamic analysis, optic fibre sensors and Acoustic Emissions (AE) acquisitions, provides a slightly invasive procedure, which is particularly targeted to historical cultural heritage. On the other hand, performing different types of acquisitions and analyses is the only way to increase the robustness of the integrity assessment. Among the different NDT's, AE has been already attempted in the past [2, 3] although a relation between the AE count and the structural integrity assessment has only recently been proposed [4, 5]. Therefore, it is useful to verify its applicability in the case of imposed differential settlement induced

doi: 10.1111/j.1475-1305.2010.00752.x

by the pier scour. During the first stage of the settlement, the AE counting has been recorded. Based on the interpretation of the AE rate, it is possible to monitor the criticality of the ongoing process. In addition, thanks to the AE equipment consisting of six AE piezoelectric transducers applied on different positions of the monitored structure, it has been possible not only to detect the ultrasonic emissions, because of crack propagations, but also to localize the main damage areas. Analysing the AE data, it is also possible to estimate the *b*-value of the Gutenberg-Richter (GR) law, allowing for the determination of the damage level into the structure. The AE and the damage evolution have been finally interpreted numerically with the aid of a finite element programme able to predict the nucleation and propagation of fracture.

The Bridge Model

The model bridge has not been obtained from a real bridge geometry, but has been designed according to historical rules for the geometry definition and shares most of the characteristics of real historical bridges. Then, according to the theory of models, the geometry has been scaled down to obtain the model dimensions. The scale of the model bridge is 1 : 2. The model bridge is 5.90 m long and 1.60 m depth. Each masonry brick is handmade and has a size of $130 \times 65 \times 30$ mm, according to the geometrical scale proportion. Strength and stiffness of masonry brick and mortar have been selected to be rather limited, to better reproduce the case of real historical bridges.

The two masonry arches of the model bridge (Figure 1) are supported by two masonry abutments and a central pier built with the same masonry. The abutments lay on concrete basements that are linked to the ground through special reinforcements.

Figure 1: Model bridge realized at the Politecnico di Torino laboratories

Above the arches, there are containment masonry walls on the four sides of the bridge, which provide the location for the filling material. The upper part of the bridge is completed with a concrete slab top, realized with limited cement content. In the central part of the bridge, above the pier, a load will be concentrated to simulate the weight of the pier foundation, which was not explicitly realized in the model.

A scheme of the model bridge is shown in Figure 2, together with the mobile steel support of the central pier that, thanks to four screws, allows for the imposition of the differential settlement. Note that the base of the pier does not lay directly on the steel plate, but on a high density polystyrene cushion, which will be removed partially during the test to simulate in the details the effect of confinement lost during the erosion process.

The density of this polystyrene support has been designed to properly correspond to the foundation soil characteristics. The exact mechanism and temporal evolution of the pier scour has been investigated numerically and experimentally (Figure 3) in collaboration with the Department of Hydraulics and Transportations of the Politecnico di Torino.

During the test, digital camera and laser scanner acquisitions have been performed. The analysis of the results suggests that a good approximation of the phenomenon is obtained providing to the model bridge pier a linear differential settlement orthogonal to the bridge longitudinal axis. The side of the pier that is hit by the river stream is subjected to the maximum settlement, whereas in correspondence of the opposite side of the pier, the settlement is vanishing.

Prior to the application of the differential settlement, it is useful to have an estimate of the model bridge mechanical response. Two aspects are of main concern: how the dynamic behaviour of the bridge will be affected and where the deformation and damage will localize. In fact, gaining those information allows for a better positioning of the measurement instruments and an optimized tuning of the acquisition resolution.

The first mechanical parameters to collect are those of the base material, i.e. the masonry. Therefore, a number of laboratory tests have been performed (Figure 4), including compression tests, diagonal compression tests, four point bending tests on masonry arches and shear tests. In addition, tests on the mortar alone and on the concrete used to support the abutments have been performed. The main mechanical parameters obtained are: the Young's modulus E, the Poisson ratio ν, the tensile strength f_t, the compressive strength f_c and the tensile fracture

doi: 10.1111/j.1475-1305.2010.00752.x

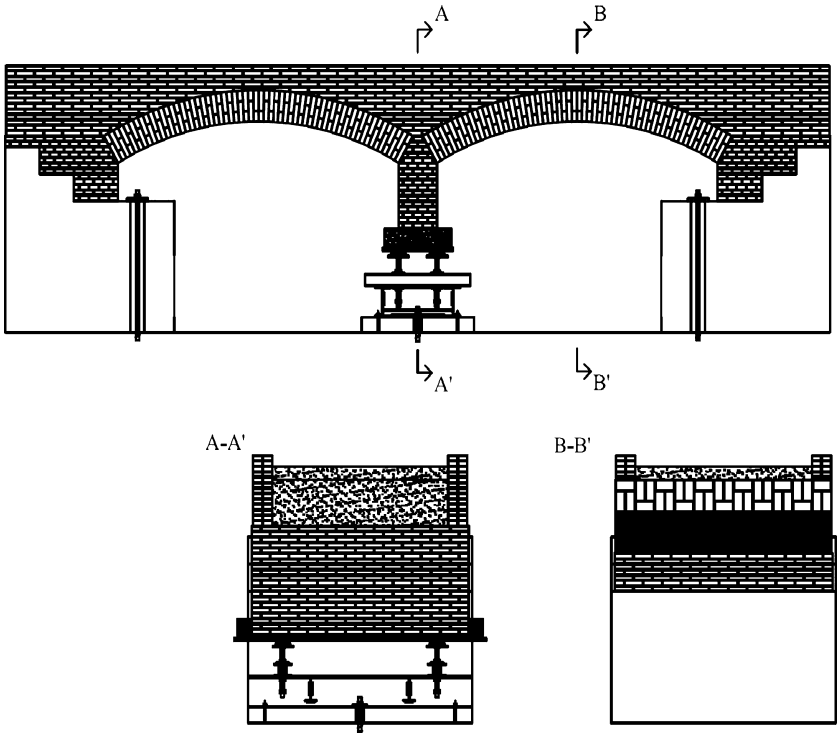

Figure 2: Lateral view and sections in correspondence of the central pier and of the mid-span

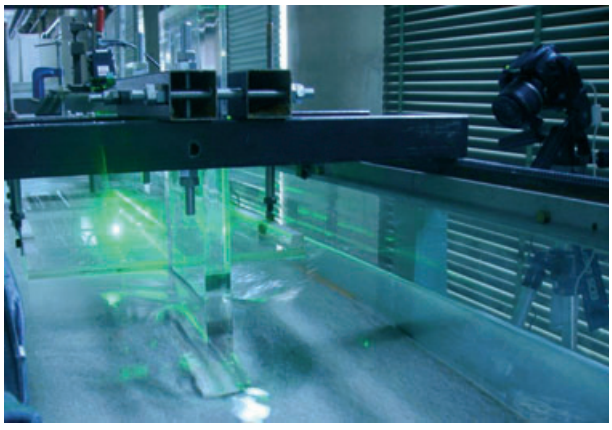

Figure 3: Experimental study of the pier scour evolution

energy G_F. These parameters are the few necessary for the numerical simulation described in the following section.

Numerical Prediction of Damage

The numerical prediction of damage has been performed developing a non-linear finite element model of the bridge with the help of the commercial code DIANA [6]. The geometry of the model accounts for all the main parts of the bridge: the masonry arches and the pier, the masonry abutment and the underlying concrete foundation, the masonry containment walls above the arches, the filling material, and, on top of the structure, the poor quality concrete slab. In addition, the polystyrene cushion below the masonry pier has been explicitly modelled, as well as the interface in correspondence of the movable support under the pier and the additional load on top of the bridge. In a first instance, the geometrical non-linearity has been disregarded. On the other hand, all the potential sources of mechanical non-linearity have

Figure 4: Laboratory tests for the mechanical characterization of the masonry: compression test (A) diagonal compression test (B) four point bending of a masonry arch (C) and shear test (D)

doi: 10.1111/j.1475-1305.2010.00752.x

been considered. To assess the damage localization in the model, a smeared crack approach was followed, both for masonry and concrete. In both cases, the adopted constitutive law is characterized by a limit compression strength and a limit tensile strength with linear softening. The simplicity of such hypothesis is preferred with respect to much more complicated material models, because very few mechanical parameters are required. The filling material, on the other hand, has been considered a very poor (i.e. with very limited stiffness) elastic material. The interface at the pier footing has a no-tension constitutive law, which allows for an explicit evaluation of the actual contact area. The mechanical parameters of the different components are shown in Table 1. The model mesh has been built with three-dimensional quadratic brick elements for the continuum part and with special quadratic interface elements for the central support. The whole model is composed of approximately 18 000 elements connected by approximately 82 000 nodes.

The load is applied in two main sequences. First, the dead load is applied together with a small uniform uplift of the central pier support. This displacement is imposed to better account for the building construction procedure and avoids the formation of spurious traction in the model, before the differential settlement is applied. In a second phase, the differential settlement with an upper bound of 20 mm is applied incrementally to the central pier. An automatic step bisection algorithm is used to improve the convergence.

The deformed mesh of the model is shown in Figure 5, where the various materials have different colours. Figure 5B is a longitudinal section of the model that shows the internal structure of the bridge.

The contours of the principal tensile stresses (Figure 6) show that the highest tractions are localized in the arches intrados close to the central pier, as well as in the extrados of the bridge (i.e. in the poor quality concrete slab) closer to the abutments. In those regions, the sensors will be localized to measure the strain (strain gages, optical strain sensors). On the other hand, linear voltage displacement transducer (LVDT) sensors will be put to monitor the pier support, to detect the decompression of the pier. High tensile tractions are also localized at the connection between the spandrel walls and the extrados of the arches, in the mid-span regions.

Table 1: Mechanical material parameters adopted in the non-linear analysis

	γ (kg m^{-3})	E (Pa)	ν	f_c (Pa)	f_t (Pa)	G_F (Nm)
Concrete	2400	$3{\cdot}10^{10}$	0.15	–	–	–
Masonry	1900	$1.5{\cdot}10^{9}$	0.2	$3{\cdot}10^{5}$	$4.3{\cdot}10^{6}$	400
Slab Concrete	2200	$5{\cdot}10^{9}$	0.15	$3{\cdot}10^{5}$	$4.3{\cdot}10^{6}$	100
Filling	2000	$5{\cdot}10^{7}$	0.49	–	–	–
Polystyrene	40	$1.01{\cdot}10^{7}$	0.2	$2.8{\cdot}10^{5}$	$4.3{\cdot}10^{6}$	10

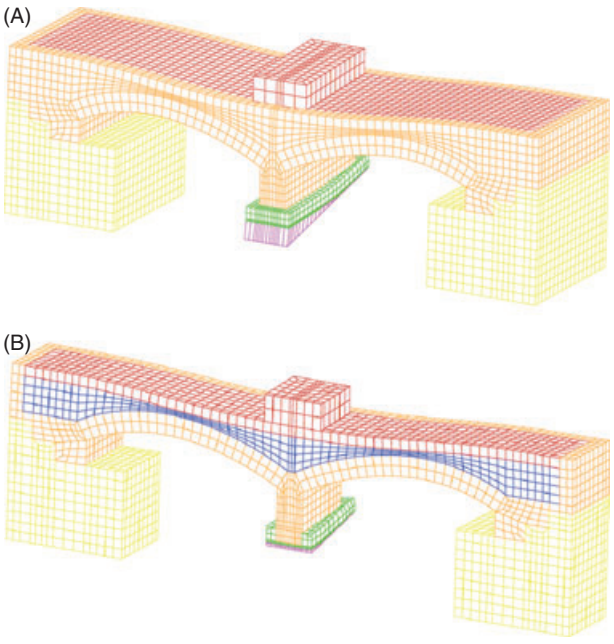

Figure 5: Deformed mesh of the complete model (A), longitudinal section of the model, showing the internal structure (B)

Figure 7 shows the contour of the minimum principal stress. It is straightforward to notice that an arch mechanism is activated between the two external abutments, which tend to hide the effect of the simulated pier scour. This phenomenon is very important and dangerous, because the overall behaviour of the bridge is made more brittle.

Thanks to the non-linear analysis, it is also possible to assess where cracks will nucleate and propagate in the model. This result is shown in Figure 8. Three main zones are detected. The first is at the masonry arches intrados, at about 0.4 m away from the central pier abutment; the crack plane is orthogonal to the bridge. The second is at the interface between the spandrel wall and the arches extrados, approximately at the mid-span of the arches; the crack plane is sub-horizontal. The third is at the concrete slab extrados right above the external abutments; the crack plane is sub-vertical. This information will help the positioning of LVDT sensors to measure the crack aperture and will be compared with the localization of the AE sources.

To provide some hints for the dynamic identification of the model, two modal analyses have also been performed. The first analysis has been carried out prior to the damage propagation. The Eigen-frequencies, shown in Table 2 and Figure 9 (left column), compare well with a preliminary experimental identification of the model.

doi: 10.1111/j.1475-1305.2010.00752.x

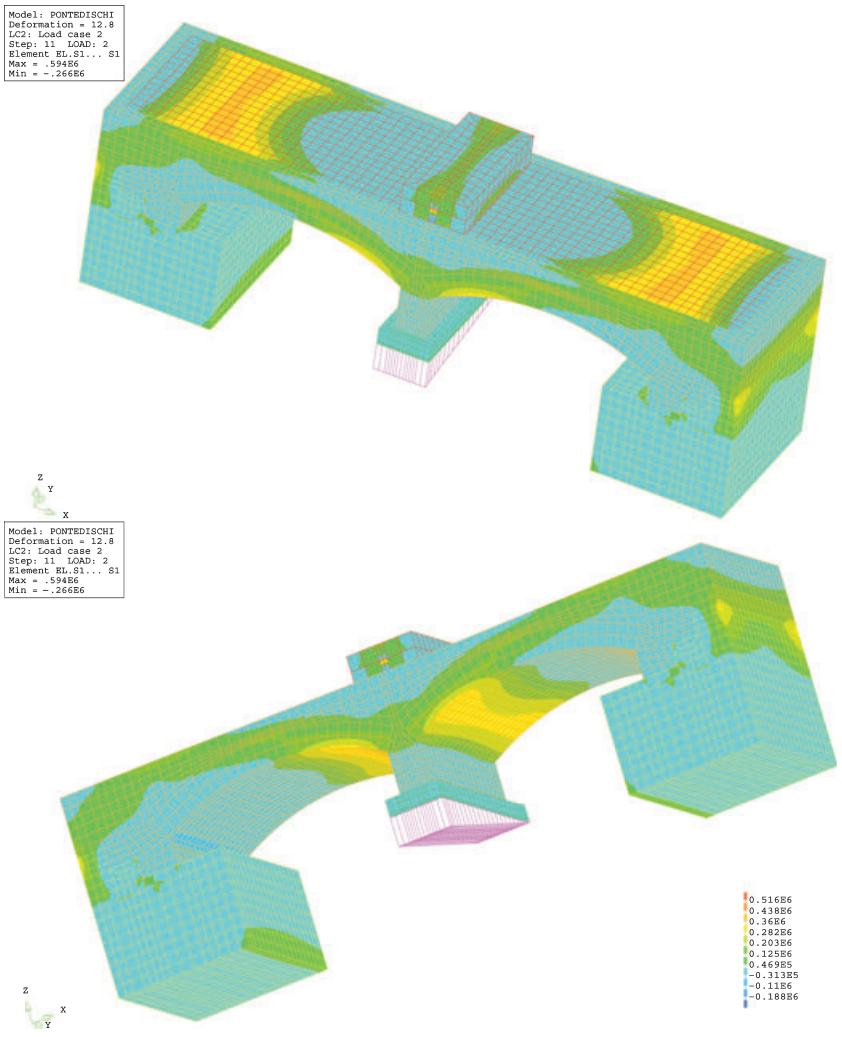

Figure 6: Tensile principal stress contours

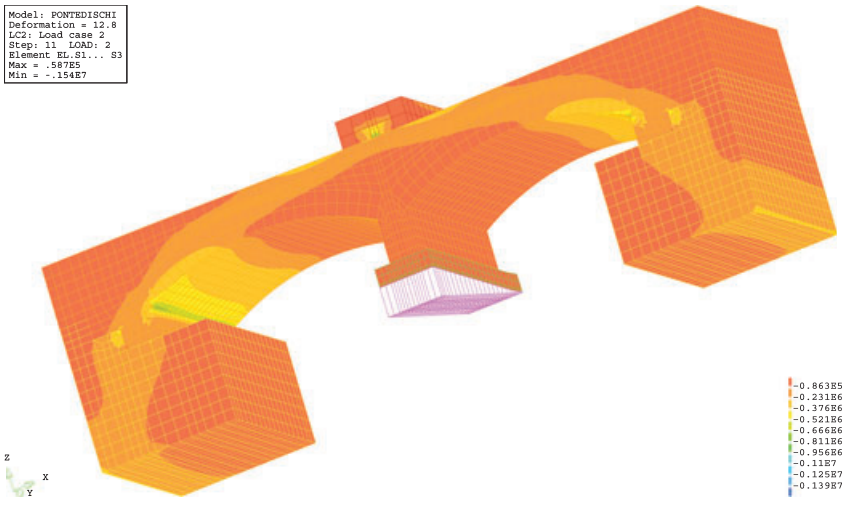

Figure 7: Compressive principal stress contour

A second analysis has been performed with the secant stiffness matrix, after the differential displacement application. This kind of analysis is basically linear and cannot account directly for the unilateral behaviour of cracks. Nevertheless, it provides us an estimate of the foreseen Eigen-frequencies shift because of damage, and then will help us in better tuning the dynamic acquisition resolution. As emphasized by the comparative results in Table 2, the effect of damage can be perceived by the experimental

doi: 10.1111/j.1475-1305.2010.00752.x

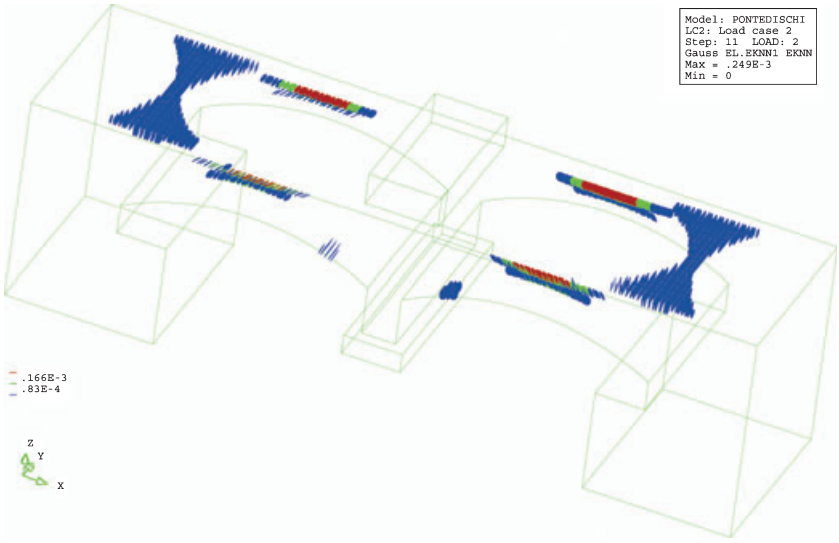

Figure 8: Smeared crack pattern corresponding to the maximum differential settlement (2 mm)

Table 2: Shift of the Eigen-frequencies because of damage propagation

	Eigen-frequency (Hz)	
Eigen-mode	Undamaged	Damaged
First	27.1	15.3
Second	32.4	25.0
Third	35.9	25.3

modal analysis. Note also that the modal shape of some of the first natural modes is also expected to change qualitatively (Figure 9).

AE Monitoring

The cracking process taking place in some portions of the masonry vault during the loading test was monitored using the AE technique. Crack advancement, in fact, is accompanied by the emission of elastic waves, which propagate within the bulk of the material. These waves can be captured and recorded by transducers applied to the surface of the structural elements.

The AE measurement system used by the authors (ATEL device) [4] consists of six piezoelectric (PZT) transducers and six control units. The PZT transducers exploit the capacity of certain crystals to produce electric signals whenever they are subjected to a mechanical stress. The ATEL sensors, acting as strainmeters, transform mechanical vibrations (AE) of about 10/7 mm amplitude into electric signals (AE signals) of about 10/6V amplitude. In the graph shown in Figure 10, the maximum sensitivity of PZT ATEL transducer is reported. The PZT transducers have a linear frequency response between 50 and 500 kHz. Considering unknown a priori the amplitude levels in the high-frequency range, the AE transducer has been selected on the basis of its great sensitivity. With the adopted equipment, the occurrences of AE events are counted. The principle of event counting is simply to count the number of times a threshold voltage A_{th} (here fixed at 100 μV to filter out the environmental noise) is exceeded by the oscillating sensor output caused by AE activity [4, 7].

The AE sensors were placed at the intrados of one of the bridge vault, to cover six almost equal competence areas (Figure 11). Thanks to the symmetry of the structure and of the loading scheme; it was possible to put limit to the AE acquisition to only one of the two vaults. This allowed for an optimized coverage with the available sensors.

As has been said, the AE transducers are sensitive to all surface vibrations lying in the frequency range between 50 and 500 kHz. This could generate a great number of received AE signals. However, because of the limits in the memory storage capacity, up to 255 counts per each period of 120 s are stored. In fact, each of the ATEL device control units is based on a 8-bit binary counter, capable to memorize a maximum number of 255 decimal events. The 120 s storage period depends on the choice of the micro-controller and its clock frequency.

This kind of approach, where only signal parameters are recorded without storing the complete waveforms, is particularly effective to carry out long-term monitoring, given the reduced number of data to be recorded and analysed.

doi: 10.1111/j.1475-1305.2010.00752.x

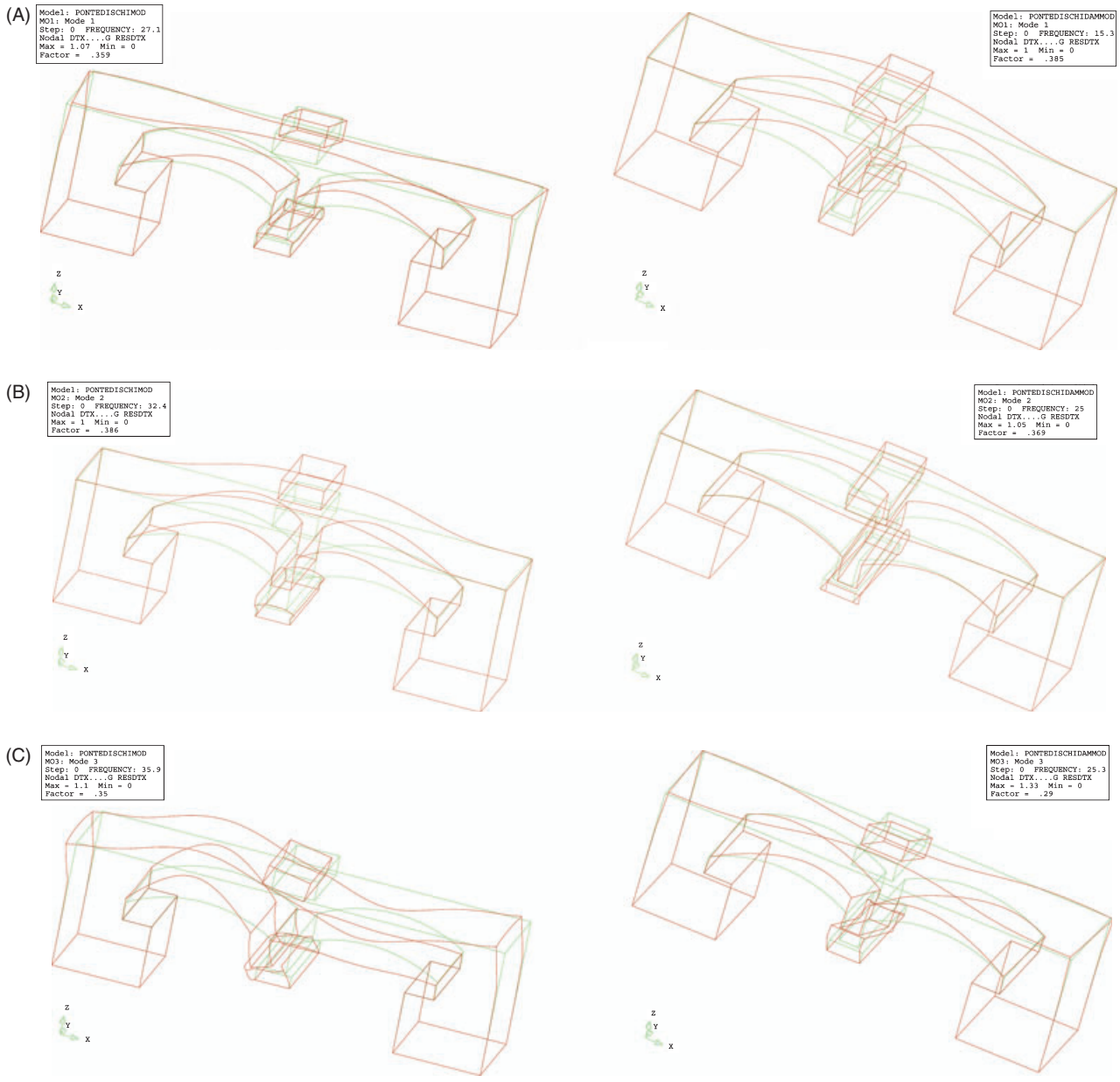

Figure 9: Modal shapes before (left) and after (above) damage propagation: first mode (A) second mode (B) and third mode (C)

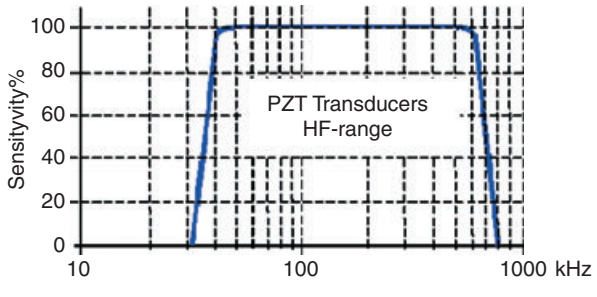

Figure 10: Frequency bands of sensitivity for the Acoustic Emissions transducers used in the acquisition

Taking into account the typical duration of an AE signal, some tens of micro-seconds, the number of counts should then correspond closely to the occurred AE events. In this procedure, referred to as Events Counting method, the number of counts (N) is obtained by determining the number of times that the signals exceed the fixed threshold voltage. Moreover, because the number of counts is proportional to crack advancement, the crack growth rate is related to the voltage amplitude of the AE elastic wave.

As reported in [7], the attenuation problem can be overcome by reducing to a few metres the distance of the transducers from the signal generation point. In this way, it can be assumed that the measurement system is able to detect the most meaningful AE events reflecting the evolution of cracking phenomena in the bridge. Utilizing the event counting method and neglecting the material attenuation properties, the AE counting number (N) can be also assumed proportional to the quantity of energy

doi: 10.1111/j.1475-1305.2010.00752.x

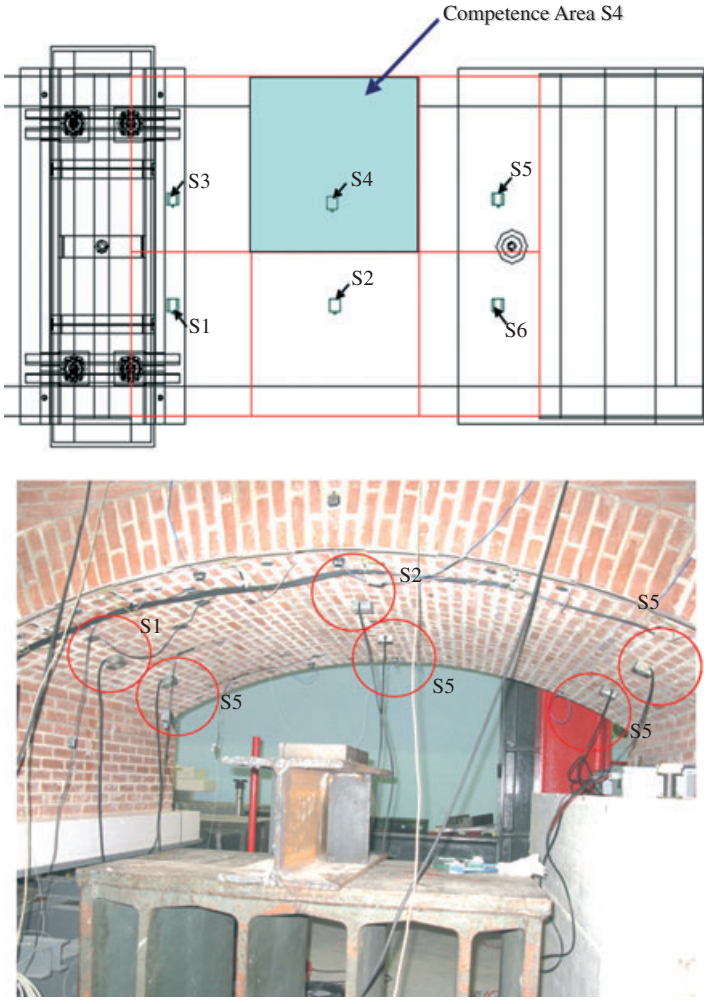

Figure 11: Positioning of the Acoustic Emissions transducers, and their competence areas

released in the masonry volumes during the loading process.

The recorded AE events are shown in Figure 12 as a function of time and compared with the stepwise application of the differential settlement. The cumulate AE curves emphasize the different amount of events in the different competence areas. These results are also displayed by shaded grey diagrams in Figure 13. The regions with the larger amount of AE counts correspond correctly to the most fractured areas visually detected.

Figure 14 shows the evolution of the AE rate as a function of the imposed displacement. The first stage presents a steeper slope, because of the extremely brittle nature of the fracture nucleation. On the other hand, the AE rate converges to a lower level as the settlement increases. This reveals a quite stable crack propagation process. It is expected that the AE rate will increase again when the system, because of the evolution of the imposed displacement, will reach a critical stage.

Besides the released energy, the events counting allows also to estimate the *b*-value of the GR law [8]. In fact, the statistical relationship between the number of AE events and their amplitude [9] is analogous to that between the number of earthquakes and their magnitude. As reported in the literature [10–14], the *b*-value systematically changes during the different stages of the failure process and tends to 1.0 approaching the final collapse, confirming the transition from diffused micro-cracking to macro-cracks that lead to the final rupture surfaces. An estimation b^* of the *b*-value is obtained by considering the cumulative distribution to the events count in a specified time window [9]:

$$b^* = \frac{\mathrm{Log}_{10} n_{\mathrm{MAX}} - \mathrm{Log}_{10}\, n_0}{\mathrm{Log}_{10} A_{\mathrm{th}}}, \qquad (1)$$

where n_{MAX} is the maximum number of AE events which can counted in a given time window, n_0 is the actual number of counts obtained during the monitoring time window and A_{th} is the AE threshold level. Therefore, the b^*-value is a sort of saturation index of the counting capability of the adopted device, and it depends on the transducers sensitivity and the fixed threshold.

doi: 10.1111/j.1475-1305.2010.00752.x

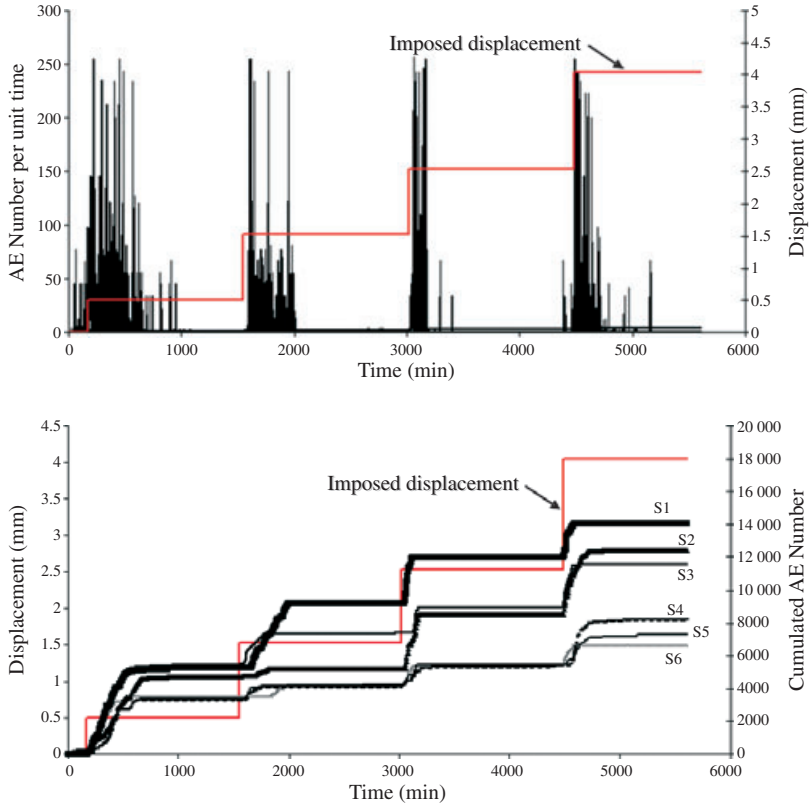

Figure 12: Acoustic Emissions rate and cumulative Acoustic Emissions as a function of time, compared with the progression of the imposed settlement

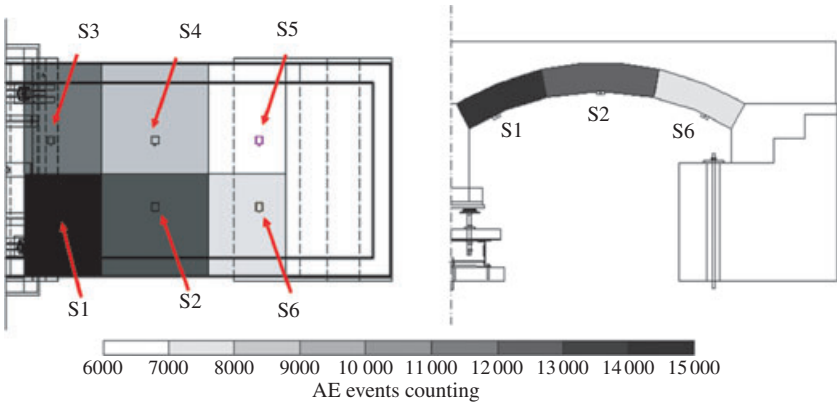

Figure 13: Number of acoustic events in each competence area

Although the two methods of calculation of the *b*-value are not directly comparable, because one requires the amplitudes of all the detected signals, while the other only the AE events count, they are complementary. In fact, as in the GR law, the evolution of the propagating cracks is well described by the transition from high *b**-values to lower *b**-values. Small values of *b** correspond to high values of n_0, indicating a large amount of AE activity, i.e. a large damage amount, whereas high values of *b** correspond to low values of n_0 indicating a small amount of AE activity, i.e. a small damage amount.

Considering the adopted monitoring system, and the threshold level $A_{th} = 100\ \mu V$, the oscillation counting limit is fixed at 255 oscillations every 120 s. In this way, the maximum number of acquirable AE events (n_{MAX}) is equal to $n \times 255$, where n is a positive integer defining the time window amplitude during the monitoring. Consequently, the *b**-value is given by [9]:

$$b^* = \frac{1}{2}[\mathrm{Log}_{10}(255n) - \mathrm{Log}_{10}n_0] \quad (2)$$

Figure 15 shows the *b**-value trend computed, considering the different phases of the imposed

Strain (2011) **47** (Suppl. 2), 158–169
doi: 10.1111/j.1475-1305.2010.00752.x

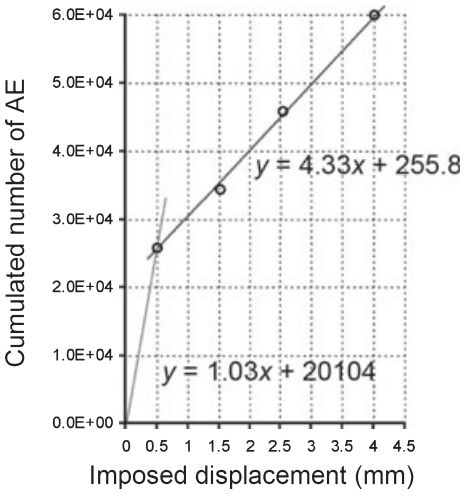

Figure 14: Evolution of the acoustic emission rate

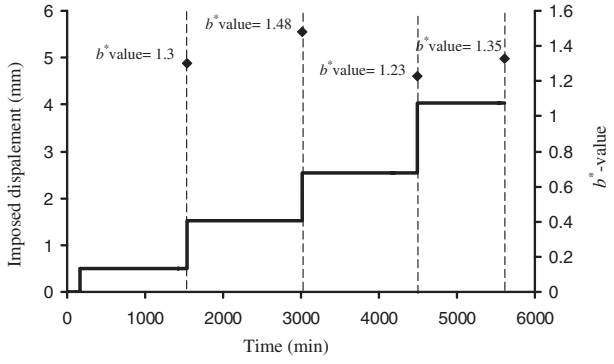

Figure 15. *b**-value trend during the incremental settlements of the pile

displacement. To consider the most significant events occurred during the monitoring process, only those exceeding 200 oscillation counts every 120 s have been taken into consideration, i.e. only the events involving higher energy content. In this way, the estimated *b**-value changes during the test between 1.23 and 1.48. These values are useful to identify the damage conditions during the crack development. The *b**-values in Figure 15 show that the monitored structure has not reached the final collapse conditions. In other terms, the damage growth in the structure is still far from the final condition, because the *b**-value attains values typical of the early stages of damage propagation. The experimental crack pattern was acquired by a careful visual inspection as well as by means of LVDT and optical fibre sensors.

Figure 16 shows that the experimental crack pattern, characterized by transversal cracking at the intrados of the vaults close to the central pier and sub-horizontal surface cracking in correspondence of the interface between the arches extrados and the spandrel walls, was correctly simulated by the numerical model (Figure 8).

Analogously to previous experiences [5, 15] of the authors, it has been recognized a strong relation among the AE locations, the experimental crack pattern and the damage zones computed by the numerical model. In particular, cracks revealed, by the visual inspection, at the arches intrados of the vaults close to the central pile are simulated in advance numerically and are detected by AE monitoring. Sensor S1 applied near the pile measured the larger amounts of AE events counts near the central pile, and the crack localizations in this zone of the vaults are correctly simulated by the numerical model (see Figures 8, 10 and 11).

On the other hand, the transversal cracking obtained numerically in the concrete slab above the

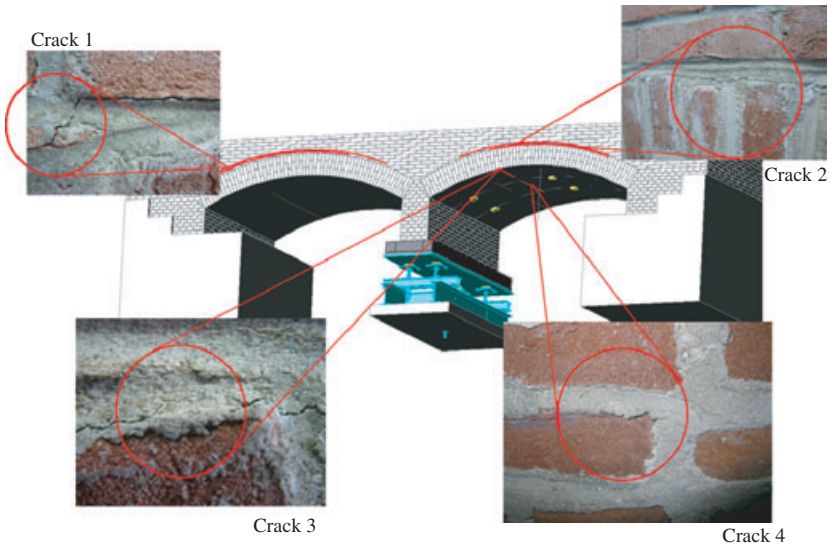

Figure 16: Comparison between the experimental and numerical crack pattern

doi: 10.1111/j.1475-1305.2010.00752.x

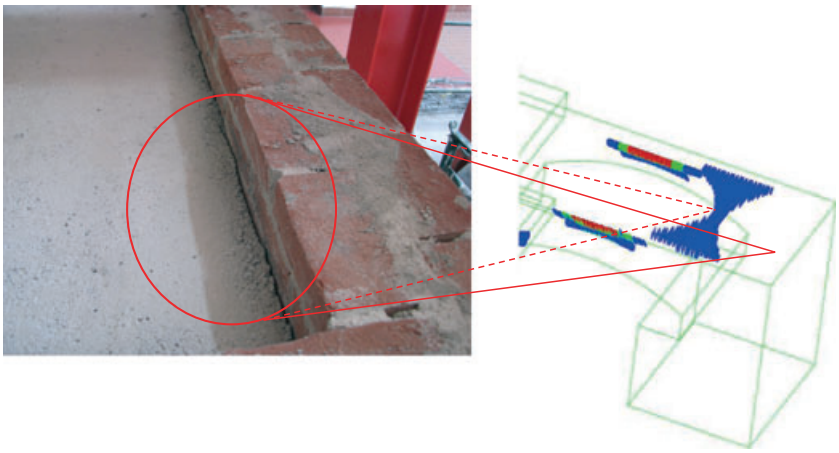

Figure 17: Detail of the detachment between the concrete slab and the masonry wall at the end of the bridge compared with the numerical previsions

filling was not detected experimentally. In place of that, a detachment between the concrete slab and the masonry wall at the end of the bridge was visible (Figure 17). The detachment is likely to be ascribed to the initial shrinkage of the poor concrete slab on top of the structure. Consequently, the AE monitoring was not able to detect it, because the AE acquisition started with the application of the differential settlement to the pier. To be able to model this phenomenon, it is necessary to model explicitly the interface between the two materials and the shrinkage of concrete.

Conclusions

A laboratory scaled model masonry bridge has been built for the experimental analysis of the pier scour phenomenon. The amount and shape of the differential settlement because of the pier scour was experimentally evaluated by means of hydraulic tests. During the application of the differential settlement, the bridge has been monitored with several non-destructive techniques, including AE. Optical fibres and dynamic identification results are still under analysis and will be reported in future works.

The numerical study of the test has been presented. Analogously to previous experiences [5, 15] of the authors, a link between the AE locations and the damage zones computed by the numerical model has been recognized. In addition, a correlation between the AE counting and the evolution of the imposed displacement has been found (Figure 12), of the same kind as the one obtained in [5], concerning a full-scale masonry vault. Finally, the monitoring of b^*-value trend has provided a quantitative assessment of the criticality of the ongoing process, revealing values which are typical of the early stages of damage propagation.

ACKNOWLEDGEMENTS

The model bridge construction as well as the dynamic acquisition and identification were performed under the MIUR grant 'Linee guida per la sorveglianza e la gestione delle strutture e infrastrutture storiche con il supporto di tecniche innovative per il monitoraggio strumentale'. The collaboration of Prof. Alessandro De Stefano and Ing. Gianluca Ruocci is gratefully acknowledged.

REFERENCES

1. Carpinteri, A. and Bocca, P. eds. (1991) *Damage and Diagnosis of Materials and Structures. Proc. of DDMS 91*, Pitagora Editrice, Politecnico di Torino, Bologna.
2. Ohtsu, M. (1996) The history and development of acoustic emission in concrete engineering. *Mag. Concrete Research*, **48**, 321–330.
3. Royles, R. and Hendry, A. W. (1991) Acoustic emission monitoring of masonry arch bridges. *Proc. Inst. Civ. Engr., Part 2*, **91**, 299–321.
4. Carpinteri, A. and Lacidogna, G. (2001) Monitoring a masonry building of the 18th century by the acoustic emission technique. *Proc. of the 7th Int. Conf. on Structural Studies, Repairs and Maintenance of Historical Buildings*, 327–337.
5. Carpinteri, A., Invernizzi, S. and Lacidogna, G. (2007) Structural assessment of a XVIIth century masonry vault with AE and numerical techniques. *Int. J. Archit. Herit.* **1** No.2, 214–226.
6. Manie, J. (2009). *DIANA – Finite Element Analysis User's Manual rel. 9.3*, TNO DIANA BV Schoemakerstraat 97, 2628 VK Delft, The Netherlands.
7. Carpinteri, A. and Lacidogna, G. (2006) Damage monitoring of an historical masonry building by the acoustic emission technique. *Mater. Struct.* **39**, 161–167.
8. Richter, C. F. (1958) *Elementary Seismology*. Freeman & Co., New York.
9. Carpinteri, A., Lacidogna, G., Niccolini, G. and Puzzi, S. (2008) Critical defect size distributions in concrete structures detected by the acoustic emission technique. *Meccanica*, **43**, 349–363.

doi: 10.1111/j.1475-1305.2010.00752.x

10. Carpinteri, A., Lacidogna, G. and Pugno, N. (2007) Structural damage diagnosis and life-time assessment by acoustic emission monitoring. *Eng. Fract. Mech.* **74**, 279–289.
11. Lemaitre, J. and Chaboche, J. L. (1990) *Mechanics of Solid Materials*. Cambridge University Press, Cambridge.
12. Colombo, S., Main, I. G. and Forde, M. C. (2003) Assessing damage of Reinforced Concrete Beam using "*b*-value" Analysis of Acoustic Emission signals. *J. Mat. Civil Engrg. (ASCE)*, **15**, 280–286.
13. Rao, M. V. M. S. and Lakschmi, P. K. J. (2005) Analysis of *b*-value and improved *b*-value of acoustic emissions accompanying rock fracture. *Curr. Sci.* Bangalore. **89**, 1577–1582.
14. Carpinteri, A., Lacidogna, G., Niccolini, G. and Puzzi, S. (2008) Morphological fractal dimension versus Power-Law exponent in the Scaling of damaged media. *Int. J. Damage Mech.* **18**, 259–282.
15. Carpinteri, A., Lacidogna, G., Invernizzi, S., Manuello, A. and Binda, L. (2008) Stability of the vertical bearing structures of the Syracuse Cathedral: experimental and numerical evaluation. *Mater. Struct.* **42**(No. 7), 877–888.

doi: 10.1111/j.1475-1305.2010.00752.x